
This is an electronic reprint of the original article.
This reprint may differ from the original in pagination and typographic detail.

Heinonen, V.; Achim, C. V.; Ala-Nissilä, Tapio

Long-wavelength properties of phase-field-crystal models with second-order dynamics

Published in:
Physical Review E

DOI:
[10.1103/PhysRevE.93.053003](https://doi.org/10.1103/PhysRevE.93.053003)

Published: 09/05/2016

Document Version
Publisher's PDF, also known as Version of record

Please cite the original version:
Heinonen, V., Achim, C. V., & Ala-Nissilä, T. (2016). Long-wavelength properties of phase-field-crystal models with second-order dynamics. *Physical Review E*, 93(5), 1-9. Article 053002.
<https://doi.org/10.1103/PhysRevE.93.053003>

Long-wavelength properties of phase-field-crystal models with second-order dynamics

V. Heinonen,^{1,*} C. V. Achim,¹ and T. Ala-Nissila^{1,2}¹COMP Centre of Excellence, Department of Applied Physics, Aalto University, School of Science, P.O. Box 11100, FI-00076, Aalto, Finland²Department of Physics, Brown University, Providence, Rhode Island 02912-1843, USA

(Received 10 March 2016; published 9 May 2016)

The phase-field-crystal (PFC) approach extends the notion of phase-field models by describing the topology of the microscopic structure of a crystalline material. One of the consequences is that local variation of the interatomic distance creates an elastic excitation. The dynamics of these excitations poses a challenge: pure diffusive dynamics cannot describe relaxation of elastic stresses that happen through phonon emission. To this end, several different models with *fast dynamics* have been proposed. In this article we use the amplitude expansion of the PFC model to compare the recently proposed hydrodynamic PFC amplitude model with two simpler models with fast dynamics. We compare these different models analytically and numerically. The results suggest that in order to have proper relaxation of elastic excitations, the full hydrodynamical description of the PFC amplitudes is required.

DOI: [10.1103/PhysRevE.93.053003](https://doi.org/10.1103/PhysRevE.93.053003)

I. INTRODUCTION

The time evolution of the microstructure of crystalline materials is mostly governed by diffusive slow phenomena. This makes materials modeling at atomistic length and timescales a demanding task. Traditional atomistic methods such as molecular dynamics have to solve the time-evolution equations at the timescale of atomistic vibrations, making it extremely difficult to extend the simulation timescales to diffusive, entropy-driven phenomena. One attempt to overcome this limitation comes with the introduction of the field theoretical framework of phase-field-crystal (PFC) models proposed by Elder *et al.* [1,2].

The main idea behind the PFC approach is that the positions of the atoms are given by an atomic number distribution function that is phenomenologically connected to the canonical distribution function of the microscopic structure. The advantage of this approach is that the positions of the atoms are taken to be thermally averaged and no need for solving the fast, atomistic timescales remains. The PFC approach has been hugely successful in describing a wide range of static and dynamical material properties [3].

One of the advantages of the PFC model is the intrinsic incorporation of elastic excitations. The PFC equations introduce an interatomic length scale that can be varied locally, giving rise to elastic excitations. This poses a challenge for the dynamics since elastic excitations should create vibrations of the lattice that cannot be described using diffusive first-order dynamics. The first attempt to tackle this problem was with the introduction of the modified PFC (MPFC) model in which a second-order time derivative is added in the time evolution equation of the system [4,5]. The MPFC model is appealing due to its simplicity and is able to introduce another timescale in the dynamics allowing for faster relaxation of elastic excitations. However, the MPFC remains hard to motivate physically and fails in describing phonon modes [6,7].

In order to describe the lattice vibrations more realistically, PFC equations have been coupled to the time evolution equation of a hydrodynamical momentum density [8]. Two main problems arise with this approach. First, the oscillating nature of the PFC solid creates spurious flows at interatomic length scale. Second, it is hard to come up with a realistic way to incorporate dissipation in the momentum density equation since macroscopic equations such as the Navier-Stokes equation consider smooth fields and it is not clear how to extend the dissipation to atomistic length scales. These problems suggest the need for a coarse graining procedure for the momentum density field.

In Ref. [9] the authors used special Fourier filters to coarse grain the velocity and the density fields that are then coupled to the microscopic density field. Another approach for smoothing out the velocity field was introduced in Ref. [10]. The authors consider a colloidal solution assuming an extreme viscosity for the colloidal particles. This way the full hydrodynamical equations are solved essentially only in the solution.

The most recent approach for coupling the momentum density with the microscopic system described in Ref. [11] uses the amplitude expansion framework of the PFC model introduced by Goldenfeld *et al.* [12,13]. The amplitude expansion of the PFC model takes advantage of the fact that the solution for the PFC density is close to a one-mode approximation of a given crystal symmetry. Instead of solving the PFC density, the amplitude equations consider the envelope of the periodically varying PFC density. This envelope is slowly varying in space making it suitable for coupling to a slowly varying velocity field.

In this article we study the difference of the amplitude description of the MPFC model and the recently proposed hydrodynamical amplitude expansion model. These are the simplest PFC models with fast dynamics. The article is organized as follows: Sec. II gives background on the PFC model and modified PFC dynamics. Amplitude expansion of the PFC model is briefly discussed and the different dynamical schemes are introduced in Sec. III. Phonon spectrum and small deformations are studied analytically in Sec. IV. The different schemes are compared numerically in Sec. V and finally the results are summarized and we conclude in Sec. VI.

*vili.heinonen@aalto.fi

II. BACKGROUND

Here we motivate the simple fast dynamics by considering linearized hydrodynamics. Let the free energy of the PFC system $F_{\text{PFC}}[n]$ be defined through PFC density n . We can write down a momentum density balance equation with the help of continuity equation for n

$$\partial_t n = -\nabla \cdot (n\mathbf{v}), \quad (1)$$

as

$$n(\partial_t \mathbf{v} + \mathbf{v} \cdot \nabla \mathbf{v}) = -n\nabla \frac{\delta F_{\text{PFC}}}{\delta n} + \mathcal{D}(n)\mathbf{v}. \quad (2)$$

Here $\delta F/\delta n$ is the chemical potential that acts as a source term for the momentum density $n\mathbf{v}$, and \mathcal{D} is some operator that defines dissipation. Assuming that velocity and its derivatives are small we can expand this equation up to the first order in \mathbf{v} , giving

$$n\partial_t \mathbf{v} = -n\nabla \frac{\delta F_{\text{PFC}}}{\delta n} + \mathcal{D}\mathbf{v}. \quad (3)$$

Taking time derivative of Eq. (1) gives

$$\partial_t^2 n = -\nabla \cdot (\mathbf{v}\partial_t n + n\partial_t \mathbf{v}),$$

from which we get

$$\begin{aligned} \partial_t^2 n &= \nabla \cdot \left[\mathbf{v}\nabla \cdot (n\mathbf{v}) + n\nabla \frac{\delta F_{\text{PFC}}}{\delta n} - \mathcal{D}\mathbf{v} \right] \\ &\approx \nabla \cdot \left[n\nabla \frac{\delta F_{\text{PFC}}}{\delta n} - \mathcal{D}\mathbf{v} \right], \end{aligned}$$

with the help of Eqs. (1) and (3). Here we have discarded nonlinear terms in \mathbf{v} . To continue with the calculation we need to define the dissipation term \mathcal{D} . For Langevin dissipation we have $\mathcal{D} = -\alpha n$, giving

$$\partial_t^2 n = \nabla \cdot \left(n\nabla \frac{\delta F_{\text{PFC}}}{\delta n} \right) + \alpha \nabla \cdot (n\mathbf{v}).$$

The latter part is given by Eq. (1) and finally the time evolution can be written in terms of n as

$$\partial_t^2 n + \alpha \partial_t n = \nabla \cdot \left(n\nabla \frac{\delta F_{\text{PFC}}}{\delta n} \right). \quad (4)$$

Often we simplify the source term by replacing the right-hand side of Eq. (4) by $\nabla^2(\delta F_{\text{PFC}}/\delta n)$, giving

$$\partial_t^2 n + \alpha \partial_t n = \nabla^2 \frac{\delta F_{\text{PFC}}}{\delta n}. \quad (5)$$

A system with dynamics described by Eq. (5) is known as the modified phase field crystal model (MPFC) [4]. Here the dissipation is controlled through the α parameter. We get the regular PFC model by taking the large α limit given by

$$\partial_t n = \nabla^2 \frac{\delta F_{\text{PFC}}}{\delta n}. \quad (6)$$

We assumed here that the velocity field \mathbf{v} and its derivatives are small. This assumption is well justified in the long wavelength regime of elastic vibrations but might break down especially in the liquid phase when advection via \mathbf{v} becomes important. Furthermore, the assumptions leading to Eq. (5) break the Galilean invariance of the system, which might be problematic in some cases. In the case of a large velocity field \mathbf{v} a hydrodynamic treatment is needed. Full coupling of the velocity field to other relevant variables will be discussed later in the article.

III. AMPLITUDE EXPANSION

In this article we use the coarse-grained PFC amplitude expansion framework [12,13]. The main idea of the amplitude expansion framework is to describe the system in terms of the envelope function of the periodic oscillations of the PFC field n . The amplitudes of the PFC oscillations are spatially uniform in the bulk liquid and solid phases relaxing the stringent requirement of a fine numerical mesh set by the spatial variation of the PFC field n . In addition to the numerical advantages of coarse-graining the PFC system, the amplitude expansion framework allows a coupling with a *smooth* hydrodynamic velocity field avoiding some difficulties faced when coupling fields that vary at an interatomic length scale to a hydrodynamic velocity field [11]. We will use such a coupling later in the article.

In the amplitude expansion framework the PFC density n is approximated by its one-mode approximation,

$$n \approx \rho + \sum_j (\eta_j e^{i\mathbf{q}_j \cdot \mathbf{r}} + \text{c.c.}), \quad (7)$$

where only the reciprocal lattice vectors \mathbf{q}_j of the first star are taken into account. Here c.c. denotes the complex conjugate. We choose a representation for a 2D hexagonal lattice as $\mathbf{q}_1 = (-\sqrt{3}/2, -1/2)$, $\mathbf{q}_2 = (0, 1)$, and $\mathbf{q}_3 = (\sqrt{3}/2, -1/2)$. Note that $|\mathbf{q}_j| = 1$. For details of the coarse-graining procedure, see Ref. [13].

The amplitudes η_j are taken to be complex to allow for displacements. Consider a change of amplitudes $\eta_j \rightarrow \eta_j \exp[-i\mathbf{q}_j \cdot \mathbf{u}(\mathbf{r})]$ with some field \mathbf{u} . The approximation for the microscopic field changes as

$$\begin{aligned} n &\approx \rho + \sum_j (\eta_j e^{-i\mathbf{q}_j \cdot \mathbf{u}} e^{i\mathbf{q}_j \cdot \mathbf{r}} + \text{c.c.}) \\ &= \rho + \sum_j (\eta_j e^{i\mathbf{q}_j \cdot (\mathbf{r} - \mathbf{u})} + \text{c.c.}). \end{aligned}$$

This shows that the field \mathbf{u} is a displacement field.

We will discuss five different models with the same free energy,

$$\begin{aligned} F = \int d\mathbf{r} \left\{ \frac{B^\ell}{2} \rho^2 - \frac{\tau}{3} \rho^3 + \frac{v}{4} \rho^4 + \frac{\tilde{B}^x}{2} |\nabla \rho|^2 + \left(\frac{\Delta B}{2} - \tau \rho + \frac{3v}{2} \rho^2 \right) A^2 + \sum_{j=1}^3 B^x |\mathcal{G}_j \eta_j|^2 \right. \\ \left. + (6v\rho - 2\tau) \left(\prod_{j=1}^3 \eta_j + \text{c.c.} \right) + \frac{3v}{4} A^4 - \frac{3v}{2} \sum_{j=1}^3 |\eta_j|^4 \right\}, \end{aligned} \quad (8)$$

where $\mathcal{P} = B^\ell - \tilde{B}^x \nabla^2$, $\mathcal{G}_j = (\nabla^2 + 2i\mathbf{q}_j \cdot \nabla)$, and $A^2 = 2 \sum_{j=1}^3 |\eta_j|^2$. These models will be described in detail in the following sections.

A. MPFC amplitude expansion (MPFCA) model

The MPFCA model is the amplitude expansion of Eq. (5). The dynamics are described by

$$\partial_t^2 \eta_j + \alpha \partial_t \eta_j = -\frac{\delta F}{\delta \eta_j^*}. \quad (9)$$

Again the dissipation happens through the term with the parameter α . The density in Eq. (8) is taken to be constant.

B. Augmented MPFC amplitude expansion (AMPFCA) model

For this model we choose a different type of dissipation term. The dynamics are described by

$$\partial_t^2 \eta_j - \alpha \mathcal{Q}_j^2 \partial_t \eta_j = -\frac{\delta F}{\delta \eta_j^*}, \quad (10)$$

where $\mathcal{Q}_j^2 = (\nabla + i\mathbf{q}_j)^2 = \nabla^2 + 2i\mathbf{q}_j \cdot \nabla - 1$.

This model can be derived from a PFC equation similar to Eq. (4) where α has been replaced with $-\alpha \nabla^2$. The amplitude representation of the Laplacian ∇^2 is \mathcal{Q}_j^2 .

This model can be examined through energetics. Let us define a kinetic energy,

$$\begin{aligned} T[\eta_j, \eta_j^*] &= \int d\mathbf{r} \left[\sum_{j=1}^3 |\partial_t \eta_j|^2 \right] \\ &= \int d\mathbf{r} \left[\sum_{j=1}^3 \partial_t \eta_j \partial_t \eta_j^* \right]. \end{aligned} \quad (11)$$

We define a total effective Hamiltonian $\mathcal{H} = T + F$. The time-evolution of the total energy becomes

$$\begin{aligned} \partial_t \mathcal{H} &= \partial_t T + \partial_t F \\ &= \int d\mathbf{r} \left[\sum_{j=1}^3 (\partial_t \eta_j^* \partial_t^2 \eta_j + \text{c.c.}) \right] \\ &\quad + \int d\mathbf{r} \left[\sum_{j=1}^3 \left(\partial_t \eta_j^* \frac{\delta F}{\delta \eta_j^*} + \text{c.c.} \right) \right] \\ &= \int d\mathbf{r} \left[\sum_{j=1}^3 \left(\partial_t \eta_j^* \partial_t^2 \eta_j + \partial_t \eta_j^* \frac{\delta F}{\delta \eta_j^*} \right) + \text{c.c.} \right] \\ &= \int d\mathbf{r} \left\{ \sum_{j=1}^3 \left[\partial_t \eta_j^* \left(\partial_t^2 \eta_j + \frac{\delta F}{\delta \eta_j^*} \right) \right] + \text{c.c.} \right\}. \end{aligned}$$

Inserting $\partial_t^2 \eta_j + \delta F / \delta \eta_j^*$ using Eq. (10) gives

$$\begin{aligned} \partial_t \mathcal{H} &= \int d\mathbf{r} \left\{ \sum_{j=1}^3 [\partial_t \eta_j^* \cdot \alpha \mathcal{Q}_j^2 \partial_t \eta_j] + \text{c.c.} \right\} \\ &= -\alpha \int d\mathbf{r} \left\{ \sum_{j=1}^3 [(\mathcal{Q}_j^* \partial_t \eta_j^*) \cdot (\mathcal{Q}_j \partial_t \eta_j)] + \text{c.c.} \right\}. \end{aligned}$$

Here we have used integration by parts. Finally, we get

$$\partial_t \mathcal{H} = -2\alpha \int d\mathbf{r} \left\{ \sum_{j=1}^3 |\mathcal{Q}_j \partial_t \eta_j|^2 \right\} \leq 0. \quad (12)$$

This shows how the parameter α controls dissipation. A similar result can be obtained for the MPFCA model with the substitution $\mathcal{Q}_j^2 \rightarrow -1$.

C. PFC amplitude expansion with hydrodynamics (HPFCA)

This model is described in depth in Ref. [11]. The dynamics are given by

$$\frac{D\mathbf{v}}{Dt} = -\nabla \frac{\delta F}{\delta \rho} - \frac{1}{\rho} \sum_{j=1}^3 \left[\eta_j^* \mathcal{Q}_j \frac{\delta F}{\delta \eta_j^*} + \text{c.c.} \right] + \frac{\mu_S}{\rho} \nabla^2 \mathbf{v} \quad (13)$$

for the velocity field,

$$\frac{d\rho}{dt} = -\nabla \cdot (\rho \mathbf{v}) + \mu_\rho \nabla^2 \frac{\delta F}{\delta \rho} + \frac{1}{2} \mu_\rho \nabla^2 (|\mathbf{v}|^2) \quad (14)$$

for the density field, and

$$\frac{d\eta_j}{dt} = -\mathcal{Q}_j \cdot (\eta_j \mathbf{v}) - \mu_\eta \frac{\delta F}{\delta \eta_j^*} \quad (15)$$

for the complex amplitudes. Here μ_S , μ_ρ , and μ_η are dissipation parameters.

D. Overdamped PFC amplitude expansion

This is the large α limit of Eq. (9). The time evolution equation becomes

$$\partial_t \eta_j = -\frac{\delta F}{\delta \eta_j^*}. \quad (16)$$

Analytically this can be realized by scaling the time as $t \rightarrow \alpha t$ in Eq. (9) and taking $\alpha \rightarrow \infty$.

E. Overdamped PFC amplitude expansion with mechanical equilibrium

For this model the dynamics of the system are given by Eq. (16) with a mechanical equilibrium constraint,

$$\frac{\delta F}{\delta \mathbf{u}}(t) = 0. \quad (17)$$

Here \mathbf{u} is the displacement field that is defined using a decomposition $\eta_j = \phi_j \exp(i\theta_j)$ as

$$\mathbf{u} = \frac{2}{3} \sum_{j=1}^3 \mathbf{q}_j \theta_j. \quad (18)$$

The details for this model can be found in Ref. [14].

IV. SMALL DISPLACEMENT LIMIT

In this section we study small long wavelength elastic displacement fields. The assumptions that we make here could be used for the full PFC description without the coarse graining procedure leading to the same calculations. This underlines another reason for using the amplitude expansion framework instead of the full PFC description, namely that the two descriptions become the same in the long-wavelength limit.¹

We assume a constant density $\rho = \rho_0$ and complex amplitudes,

$$\eta_j = \phi_0 \exp[-i\mathbf{q}_j \cdot \mathbf{u}(\mathbf{r}, t)], \quad (19)$$

where \mathbf{u} is a displacement field that is assumed to be small. More specifically the displacement field is expanded up to linear order in the dynamical equations and up to quadratic order in the energy. We also assume that \mathbf{u} is *slowly varying* and take a long-wavelength limit discarding all the derivatives higher than the second order. Expanding the energy up to second order in \mathbf{u} gives an elastic energy,

$$F_{\text{el}} = \int d\mathbf{r} \left(\frac{1}{2} \boldsymbol{\sigma} : \boldsymbol{\epsilon} \right), \quad (20)$$

where

$$\boldsymbol{\epsilon} = \frac{1}{2} [\nabla \mathbf{u} + (\nabla \mathbf{u})^T] \quad (21)$$

is the linear strain tensor and

$$\boldsymbol{\sigma} = 3B^x \phi_0^2 [2\boldsymbol{\epsilon} + (\nabla \cdot \mathbf{u})\mathbf{I}] \quad (22)$$

is the linear elastic stress tensor. The elastic constants can be extracted from a linear relationship $\sigma_{ij} = C_{ijkl}\epsilon_{kl}$ and are those of a 2D hexagonal crystal symmetry. See Appendix A for the derivation of Eq. (20).

Some results are needed in order to continue with the analysis:

$$\begin{aligned} \frac{\delta F}{\delta u_k} &= \sum_j \left(\frac{\partial \eta_j^*}{\partial u_k} \frac{\delta F}{\delta \eta_j^*} + \text{c.c.} \right) = \sum_j \left(i q_{j,k} \eta_j^* \frac{\delta F}{\delta \eta_j^*} + \text{c.c.} \right) \\ &= 2 \sum_j \text{Re} \left(i q_{j,k} \eta_j^* \frac{\delta F}{\delta \eta_j^*} \right) = -2 \sum_j \text{Im} \left(q_{j,k} \eta_j^* \frac{\delta F}{\delta \eta_j^*} \right). \end{aligned}$$

Here u_k is the k th component of \mathbf{u} and $q_{j,k}$ is the k th component of \mathbf{q}_j . Using a different notation we write

$$\frac{\delta F}{\delta \mathbf{u}} = -2 \sum_j \text{Im} \left(\mathbf{q}_j \eta_j^* \frac{\delta F}{\delta \eta_j^*} \right). \quad (23)$$

We have for all the linear differential operators \mathcal{L} without a constant part a following identity:

$$\mathcal{L}(\phi_0 e^{-i\mathbf{q}_j \cdot \mathbf{u}}) = -(i\phi_0 \mathbf{q}_j \cdot \mathcal{L} \mathbf{u}) e^{-i\mathbf{q}_j \cdot \mathbf{u}} + \mathcal{O}(|\mathbf{u}|^2). \quad (24)$$

¹The similarity is based on an assumption of an one-mode approximation for the PFC density n with a small displacement field. This approximation should be accurate in the long-wavelength limit.

Another identity that we need is

$$\sum_{j=1}^3 \mathbf{q}_j \otimes \mathbf{q}_j = \frac{3}{2} \mathbf{I}, \quad (25)$$

i.e., the sum of the dyadic of the reciprocal lattice vectors sums up to a constant times identity.

It should also be pointed out that in the linear regime the functional derivative of the free energy with respect to the displacement field can be approximated as

$$\frac{\delta F}{\delta \mathbf{u}} \approx \frac{\delta F_{\text{el}}}{\delta \mathbf{u}} = -3B^x \phi_0^2 \mathbf{u}^\sharp, \quad (26)$$

where $\mathbf{u}^\sharp = \nabla^2 \mathbf{u} + 2\nabla \nabla \cdot \mathbf{u}$.

A. MPFCA

Inserting Eq. (19) in Eq. (9) gives

$$-i\mathbf{q}_j \cdot (\partial_t^2 \mathbf{u} + \alpha \partial_t \mathbf{u}) \phi_0 e^{-i\mathbf{q}_j \cdot \mathbf{u}} = -\frac{\delta F}{\delta \eta_j^*}$$

in the linear displacement regime. Multiplying by $\mathbf{q}_j \eta_j^*$ on both sides, taking the imaginary part and summing over j gives

$$-\phi_0^2 \left(\sum_{j=1}^3 \mathbf{q}_j \otimes \mathbf{q}_j \right) \cdot (\partial_t^2 \mathbf{u} + \alpha \partial_t \mathbf{u}) = -\sum_{j=1}^3 \mathbf{q}_j \text{Im} \left(\eta_j^* \frac{\delta F}{\delta \eta_j^*} \right),$$

which becomes

$$\partial_t^2 \mathbf{u} + \alpha \partial_t \mathbf{u} = -\frac{1}{3} \phi_0^{-2} \frac{\delta F}{\delta \mathbf{u}} \quad (27)$$

with the help of Eq. (25).

Using Eq. (26) we can write this as

$$\partial_t^2 \mathbf{u} + \alpha \partial_t \mathbf{u} = B^x \mathbf{u}^\sharp. \quad (28)$$

This can be solved with an ansatz $\mathbf{u} = \mathbf{u}_0 \exp(-\omega t + i\mathbf{k} \cdot \mathbf{r})$. These plane-wave solutions can be decomposed into a parallel part $\mathbf{u}_\parallel \exp(-\omega_\parallel t + i\mathbf{k} \cdot \mathbf{r})$, where $\mathbf{k} \cdot \mathbf{u}_\parallel = k u_\parallel$ and into a perpendicular part $\mathbf{u}_\perp \exp(-\omega_\perp t + i\mathbf{k} \cdot \mathbf{r})$, where $\mathbf{k} \cdot \mathbf{u}_\perp = 0$. The general plane-wave solution to Eq. (28) is a superposition of these to components with different values of \mathbf{k} .

Let us solve for the perpendicular mode. Inserting the ansatz into Eq. (28) gives

$$\omega_\perp^2 - \alpha \omega_\perp = -B^x k^2, \quad (29)$$

which can be solved for ω_\perp as

$$\omega_\perp = \frac{1}{2} \alpha \pm \frac{i}{2} \sqrt{4B^x k^2 - \alpha^2}, \quad (30)$$

when

$$k > k_c = \frac{\alpha}{2\sqrt{B^x}}. \quad (31)$$

Here k_c is the critical k value. If this does not hold we get

$$\omega_\perp = \frac{1}{2} \alpha \pm \frac{1}{2} \sqrt{\alpha^2 - 4B^x k^2}. \quad (32)$$

The calculation for the longitudinal modes gives

$$\omega_\parallel = \frac{1}{2} \alpha \pm \frac{i}{2} \sqrt{12B^x k^2 - \alpha^2}, \quad (33)$$

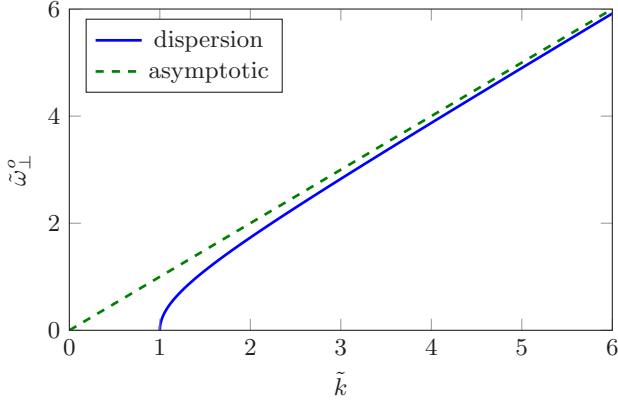


FIG. 1. The dispersion relation for the oscillating part $\omega_\perp^\circ = \text{Im}(\omega_\perp)$ for the MPFCA model given by Eq. (30). The units are rescaled as $\tilde{k} = 2\sqrt{3}B^x k/\alpha$ and $\tilde{\omega}_\perp^\circ = 2\omega_\perp^\circ/\alpha$.

with a critical k value,

$$k_c = \frac{\alpha}{2\sqrt{3}B^x}. \quad (34)$$

The dispersion relation for the oscillating part is shown in Fig. 1.

B. AMPFCA

Repeating the previous calculation we get

$$\partial_t^2 \mathbf{u} + \alpha(-\nabla^2 + 1)\partial_t \mathbf{u} = B^x \mathbf{u}^\sharp, \quad (35)$$

resembling Eq. (28). Here the imaginary part gives a condition $\nabla \cdot \mathbf{u} = 0$, which is equivalent to the assumption that $\phi_j = \phi_0$ are constant. For details see Appendix B.

From here on the only difference in the calculation is the extra $-\alpha \nabla^2$. This contributes an extra k^2 in the final result that can be obtained by replacing α in the previous calculation with $\alpha(1 + k^2)$. This gives

$$\omega_\perp = \frac{1}{2}\alpha(1 + k^2) \pm \frac{i}{2}\sqrt{4B^x k^2 - (1 + k^2)^2 \alpha^2} \quad (36)$$

for the transversal modes subject to the condition

$$\begin{aligned} \frac{2B^x}{\alpha^2} - 1 - 2\frac{\sqrt{B^x}}{\alpha}\sqrt{\frac{B^x}{\alpha^2} - 1} &< k^2 \\ &< \frac{2B^x}{\alpha^2} - 1 + 2\frac{\sqrt{B^x}}{\alpha}\sqrt{\frac{B^x}{\alpha^2} - 1}. \end{aligned} \quad (37)$$

For the longitudinal modes we get

$$\omega_\parallel = \frac{1}{2}\alpha(1 + k^2) \pm \frac{i}{2}\sqrt{12B^x k^2 - (1 + k^2)^2 \alpha^2}, \quad (38)$$

subject to the condition

$$\begin{aligned} \frac{6B^x}{\alpha^2} - 1 - 2\frac{\sqrt{3B^x}}{\alpha}\sqrt{\frac{3B^x}{\alpha^2} - 1} &< k^2 \\ &< \frac{6B^x}{\alpha^2} - 1 + 2\frac{\sqrt{3B^x}}{\alpha}\sqrt{\frac{3B^x}{\alpha^2} - 1}. \end{aligned} \quad (39)$$

The dispersion relation for the oscillating part is shown in Fig. 2.

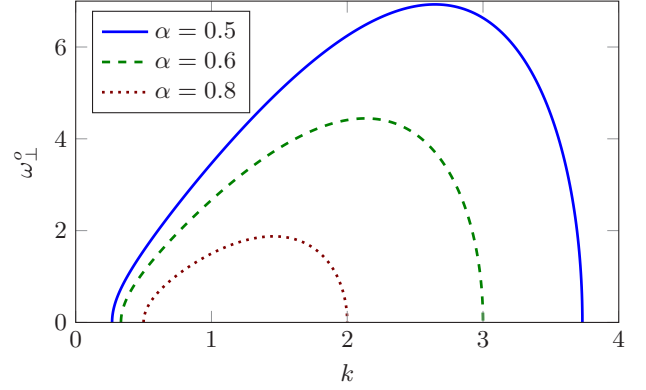


FIG. 2. The dispersion relation for the oscillating part $\omega_\perp^\circ = \text{Im}(\omega_\perp)$ for the AMPFCA model with several different α given by Eq. (36). Here $B^x = 1$.

C. HPFCA

Equation (15) can be written for the displacement field \mathbf{u} with the help of Eqs. (23) and (25) as

$$\partial_t \mathbf{u} + \mathbf{v} \cdot \nabla \mathbf{u} \approx \partial_t \mathbf{u} = \mathbf{v} - \frac{1}{2}\phi_0^{-2}\mu_\eta \frac{\delta F_{\text{el}}}{\delta \mathbf{u}} = \mathbf{v} + \mu_\eta B^x \mathbf{u}^\sharp. \quad (40)$$

The equation for the velocity field, Eq. (13), becomes

$$\begin{aligned} \underbrace{\partial_t \mathbf{v} + \mathbf{v} \cdot \nabla \mathbf{v}}_{\approx \partial_t \mathbf{v}} &= -\frac{1}{\rho_0} \sum_{j=1}^3 \left[\eta_j^* \mathcal{Q}_j \frac{\delta F}{\delta \eta_j^*} + \text{c.c.} \right] + \frac{\mu_s}{\rho_0} \nabla^2 \mathbf{v} \\ &\approx -\frac{2}{\rho_0} \sum_{j=1}^3 \text{Re} \left[\eta_j^* i \mathbf{q}_j \frac{\delta F}{\delta \eta_j^*} \right] + \mu_s \rho_0^{-1} \nabla^2 \mathbf{v} \\ &= \frac{2}{\rho_0} \sum_{j=1}^3 \text{Im} \left[\eta_j^* \mathbf{q}_j \frac{\delta F}{\delta \eta_j^*} \right] + \mu_s \rho_0^{-1} \nabla^2 \mathbf{v} \\ &\approx -\frac{1}{\rho_0} \frac{\delta F_{\text{el}}}{\delta \mathbf{u}} + \mu_s \rho_0^{-1} \nabla^2 \mathbf{v} \\ &= 3B^x \rho_0^{-1} \phi_0^2 \mathbf{u}^\sharp + \mu_s \rho_0^{-1} \nabla^2 \mathbf{v}. \end{aligned} \quad (41)$$

Here we assume $\nabla(\delta F/\delta \eta_j^*) \approx 0$, since it produces terms with derivatives of the displacement field with a degree higher than two.

Let $\hat{\xi}$ be the Fourier transform of a vector field ξ subject to the condition $\xi = \int d\mathbf{k} [\exp(i\mathbf{k} \cdot \mathbf{r}) \hat{\xi}(\mathbf{k})]$. We can rewrite Eq. (41) as

$$\partial_t \hat{v} = 3B^x \rho_0^{-1} \phi_0^2 \hat{u}^\sharp - \mu_s \rho_0^{-1} k^2 \hat{v}, \quad (42)$$

from which we can solve

$$\partial_t (\hat{v} e^{\mu_s \rho_0^{-1} k^2 t}) = 3B^x \rho_0^{-1} \phi_0^2 \hat{u}^\sharp. \quad (43)$$

Now we can write Eq. (40) in Fourier space as

$$\partial_t \hat{u} = \hat{v} + \mu_\eta B^x \hat{u}^\sharp. \quad (44)$$

Multiplying both sides by $\exp(\mu_s \rho_0^{-1} k^2 t)$ and taking the time derivative gives

$$\begin{aligned} \partial_t [(\partial_t \hat{u}) e^{\mu_s \rho_0^{-1} k^2 t}] \\ = \partial_t (\hat{v} e^{\mu_s \rho_0^{-1} k^2 t}) + \mu_\eta B^x \partial_t (\hat{u}^\sharp e^{\mu_s \rho_0^{-1} k^2 t}), \end{aligned} \quad (45)$$

resulting in

$$\partial_t^2 \hat{u} + \mu_S \rho_0^{-1} k^2 \partial_t \hat{u} = 3B^x \rho_0^{-1} \phi_0^2 \hat{u}^\sharp + \mu_\eta B^x (\partial_t \hat{u}^\sharp + \mu_S \rho_0^{-1} k^2 \hat{u}^\sharp), \quad (46)$$

with the help of Eq. (43). The Fourier transform \hat{u}^\sharp is given by

$$\hat{u}^\sharp = -k^2 \hat{u} - 2\mathbf{k}\mathbf{k} \cdot \hat{u}. \quad (47)$$

Let us split \hat{u} into two orthogonal parts subject to $\hat{u} = \hat{u}_\perp + \hat{u}_\parallel$ and $\mathbf{k} \cdot \hat{u}_\perp = 0$. For transversal modes $\hat{u}^\sharp = -k^2 \hat{u}_\perp$, giving

$$\partial_t^2 \hat{u}_\perp + (\mu_S \rho_0^{-1} + \mu_\eta B^x) k^2 \partial_t \hat{u}_\perp + 3B^x k^2 (\rho_0^{-1} \phi_0^2 + \frac{1}{3} \mu_\eta \mu_S \rho_0^{-1} k^2) \hat{u}_\perp = 0. \quad (48)$$

This can be solved with the ansatz $\hat{u}_\perp = \exp(-\omega_\perp t)$, giving

$$\omega_\perp^2 - (\mu_S \rho_0^{-1} + \mu_\eta B^x) k^2 \omega_\perp + 3B^x k^2 (\rho_0^{-1} \phi_0^2 + \frac{1}{3} \mu_\eta \mu_S \rho_0^{-1} k^2) = 0. \quad (49)$$

We solve this for ω_\perp^2 resulting in

$$\omega_\perp = \frac{1}{2} k^2 (\mu_S \rho_0^{-1} + \mu_\eta B^x) \pm i \frac{k}{2} \sqrt{12B^x \phi_0^2 \rho_0^{-1} - (\mu_S \rho_0^{-1} - B^x \mu_\eta)^2 k^2}, \quad (50)$$

which we can divide into an oscillating part,

$$\omega_\perp^o = \frac{k}{2} \sqrt{12B^x \phi_0^2 \rho_0^{-1} - (\mu_S \rho_0^{-1} - B^x \mu_\eta)^2 k^2}, \quad (51)$$

and a damping part,

$$\omega_\perp^d = \frac{1}{2} k^2 (\mu_S \rho_0^{-1} + \mu_\eta B^x), \quad (52)$$

subject to the condition $\omega_\perp = \omega_\perp^d + i\omega_\perp^o$. The existence of the oscillating solutions is subject to the condition

$$k < \frac{\sqrt{12B^x \phi_0^2 \rho_0^{-1}}}{|\mu_S \rho_0^{-1} - B^x \mu_\eta|} \phi_0. \quad (53)$$

Those modes for which this does not hold are damped with a damping coefficient

$$\omega_\perp^d = \frac{1}{2} k^2 (\mu_S \rho_0^{-1} + \mu_\eta B^x) \pm \frac{k}{2} \sqrt{(\mu_S \rho_0^{-1} - B^x \mu_\eta)^2 k^2 - 12B^x \phi_0^2 \rho_0^{-1}}, \quad (54)$$

where the sign is determined by the initial velocity. The dispersion relation for the oscillating component is shown in Fig. 3.

A similar calculation gives an oscillating solution

$$\omega_\parallel = \frac{1}{2} k^2 (\mu_S \rho_0^{-1} + 3\mu_\eta B^x) \pm i \frac{k}{2} \sqrt{36B^x \phi_0^2 \rho_0^{-1} - (\mu_S \rho_0^{-1} - 3B^x \mu_\eta)^2 k^2}, \quad (55)$$

for the longitudinal modes.

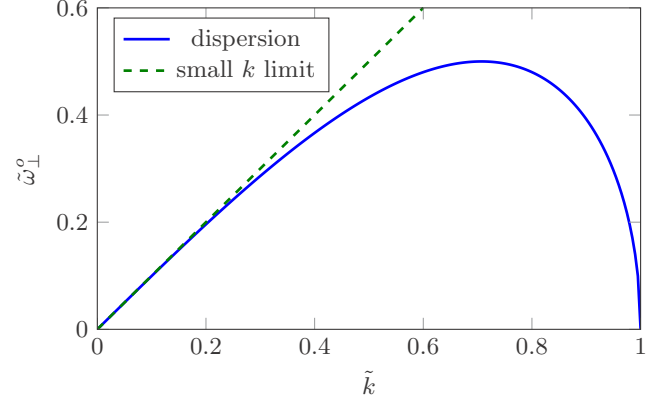


FIG. 3. The dispersion relation $\tilde{\omega}_\perp^o(\tilde{k}) = \tilde{k} \sqrt{1 - \tilde{k}^2}$ for the oscillating component of the perpendicular wave in the linear displacement limit for the HPFCA model. Here $\tilde{\omega}_\perp^o = |\mu_S - \frac{3}{2} B^x \mu_\eta \rho_0| \omega_\perp^o / (6B^x \phi_0^2)$ and $\tilde{k}^2 = (\mu_S - \frac{3}{2} B^x \rho_0 \mu_\eta)^2 k^2 / (12B^x \phi_0^2 \rho_0)$.

V. NUMERICAL RESULTS

The numerical results for the AMPFCA model given by the tests presented here were practically indistinguishable from the MPFCA results. For this reason, the AMPFCA results are not presented here separately. This will be discussed further in Sec. VI.

A. Numerical study of small deformations

We studied the time evolution of longitudinal waves of the form $\mathbf{u}(x) = a \sum_{m=1}^{128} [\sin(2\pi m x / L_x) / m^2]$, where L_x is the size of the periodic box in x dimension and a is the nearest-neighbor distance $4\pi/\sqrt{3}$.² The calculations were performed in a rectangular box with periodic boundary conditions. The dimensions of the box were $(L_x, L_y) = (8192, 256)$. Note that the displacement field varies only in one direction reducing the system to one dimension. Here we use a parametrization $\alpha = 0.05$, $\mu_S = 0$, $\mu_\rho = 0.05$, $\mu_\eta = 1$, $B^x = \tilde{B}^x = 1$, $\Delta B = 0.097$, $\tau = 0.885$, $\nu = 1$ and the average density $\rho_0 = 0.1$. For the numerical discretization we used $\Delta x = \Delta y = 4$ and the time step Δt was varied from 0.0625 to 0.125. For more on numerical details see Appendix C.

The results are presented in Figs. 4 and 5. For the MPFCA model there is a critical wave vector k_c below which no oscillating solutions exist. It can also be seen that the oscillating solutions above k_c are damped at a rate that is independent of k . The HPFCA model behaves very differently showing oscillating solutions for all k and damping dependent on k .

B. Grain rotation

In order to compare the different dynamics, we solve the time evolution of a circular grain embedded in a crystalline matrix. This numerical test is simple but nontrivial and should provide insight into the difference of the dynamical schemes discussed in this article.

²Any waveform with a large number of modes would do since the modes are not coupled in the linear regime.

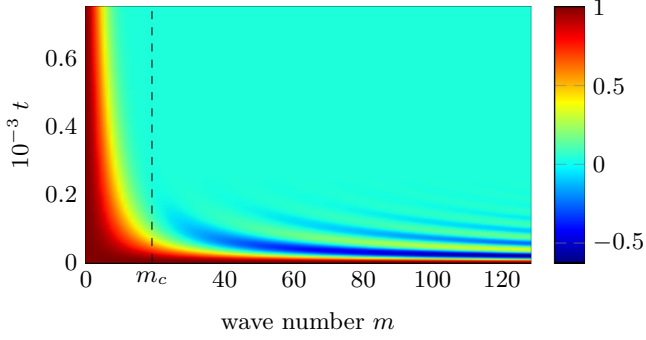


FIG. 4. The spectrum of the MPFCA model as a function of time. The color shows the relative amplitude of the m th mode at a given time. The amplitudes are scaled to unity at time zero. The wave number m denotes the m th harmonic. The wave vectors can be recovered as $k_m = 2\pi m/L_x$. The analytical cutoff for the oscillating solutions is shown here at wave number m_c .

The grain is tilted by an angle $\gamma(t=0)$ creating a mismatch at the perimeter of the grain, which gives rise to a grain boundary. The setting is shown in Fig. 6.

Assuming that the grain boundary motion is curvature driven, i.e., $v_\perp = \partial_t R \sim \kappa = R^{-1}$, we can solve for the time evolution of the radius $R(t)$ giving $\partial_t(R^2) = \text{constant}$. This implies that the area of the grain decreases linearly. Note that if the normal velocity of the grain boundary is proportional to the curvature of the grain boundary, the time evolution of a circular grain is self similar in the sense that the grain will be circular also at later times.

At small angles the number of the dislocation cores n_d at the perimeter of the rotated grain is proportional to the rotation angle and the length of the boundary. This can be written as $n_d \sim \gamma(t)R(t)$. Dislocation cores repel each other and annihilate in the very end of the calculation. For earlier times n_d is constant in time implying that $\gamma(t) \sim R^{-1}$. From this it follows that angle γ increases as radius R decreases. The dynamics of this type of rotated grain is discussed in depth in Ref. [15].

The results of the grain rotation calculations are shown in Fig. 7. All the different realizations show linear time evolution

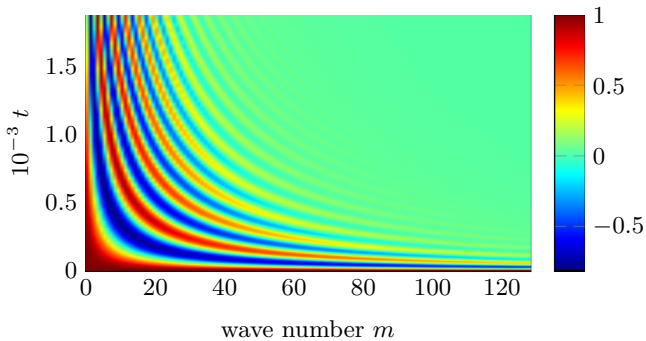


FIG. 5. The spectrum of the HPFCA model as a function of time. The color shows the relative amplitude of the m th mode at a given time. The amplitudes are scaled to unity at zero. The wave number m denotes the m th harmonic. The wave vectors can be recovered as $k_m = 2\pi m/L_x$. The time difference between the peaks scales with the wave number as m^{-2} since the dissipation rate is proportional to k^2 .

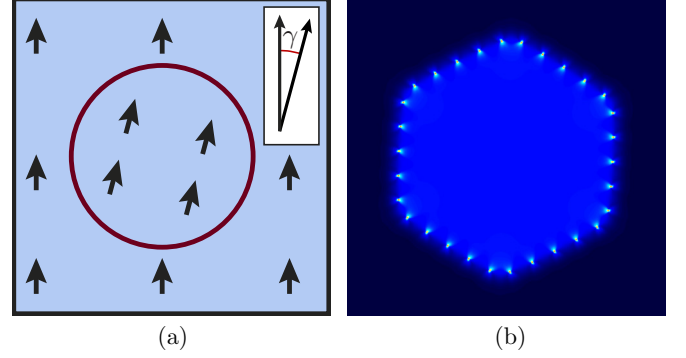


FIG. 6. (a) Schematic of the grain rotation calculation: the grain is rotated by an angle γ (the angle difference is shown in the inset). (b) The magnitude of the gradient of the displacement field $|\nabla \mathbf{u}|$ from a calculation showing the dislocation cores at the perimeter of the grain. The uniform brighter color inside the grain is due to the angle difference γ .

for the area of the rotated grain. The behavior of the MPFCA model reduces to the overdamped amplitude model when $\alpha = 1$. More interestingly, the trajectory for the MPFCA model converges to the one obtained with $\alpha = 0.1$. Decreasing α further did not make the dynamics faster. The HPFCA model gives the same trajectory as the mechanically equilibrated overdamped model as already discovered in Ref. [11].

The parameters used for these calculations were $\mu_s = 0$, $\mu_\rho = 0.05$, $\mu_\eta = 1$, $B^x = \tilde{B}^x = 1$, $\Delta B = 0.097$, $\tau = 0.885$, $\nu = 1$ and the average density $\rho_0 = 0.1$.

The calculations were performed in a box of a size $L_x = L_y = 1536$ with a discretization $\Delta x = \Delta y = 2$, $\Delta t = 0.125$. For more details see Appendix C.

VI. SUMMARY AND CONCLUSION

We have analyzed three different schemes for the time evolution of the PFC amplitude system analytically and numerically. We have shown that no true phonons exist for

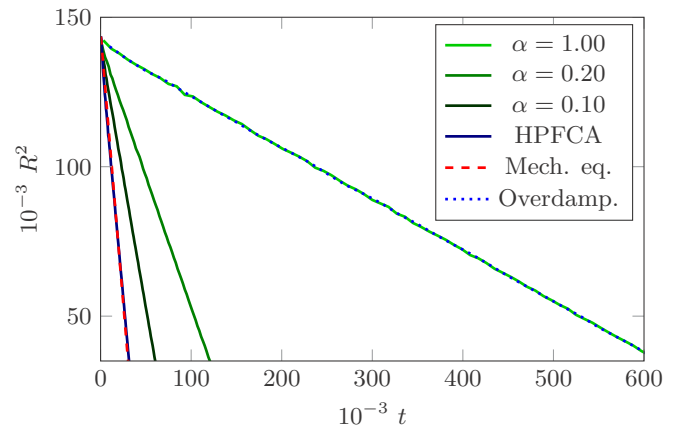


FIG. 7. The squared radii of the shrinking circular grain with different models and parametrization. The overdamped model and MPFCA with $\alpha = 1$ give the slowest dynamics. MPFCA dynamics becomes faster with decreasing α but cannot reach the fastest trajectories given by the mechanically equilibrated model and the HPFCA model.

other models than the HPFCA model. The analytical results for the small displacements are verified numerically showing that the damping of the oscillating solutions for the MPFCA model dissipate at the same rate regardless of the wavelength and that there is a critical wavelength over which the waves do not oscillate. All the different modes of the HPFCA model oscillate and the dissipation is proportional to k^2 .

The grain rotation experiment shows that in case of the MPFCA model, there is a critical value for the dissipation parameter α below which the dynamics does not get faster. Unlike for the HPFCA model, the limiting trajectory is not that of the mechanically equilibrated system. Instead, slower time evolution is seen. This behavior should not be caused by the cutoff in the oscillating solutions since k_c can be controlled by decreasing α allowing all the modes in the periodic box to oscillate. Instead, it is likely that this behavior follows from the fact that the parameter α controls all the dissipation in the system. Even if the oscillating modes are damped less allowing for reducing the energy through the displacement field, the overall dissipation is reduced hindering the diffusional relaxation of the system. Taking μ_S to 0 for the HPFCA model does not affect the diffusional dissipation that happens through the parameter μ_η .

The AMPFCA results are not shown in the numerical experiments since they are indistinguishable from the results given by the MPFCA model. It seems that at large α both models collapse into the overdamped case and at low α they become the same. Studying the small displacement dispersion relations of these two models can give some insight into why this happens. Let us consider Eqs. (30) and (36). Expanding the dispersion relation up to a quadratic order in both α and k Eq. (36) becomes

$$\begin{aligned}\omega_\perp &= \frac{1}{2}\alpha + \mathcal{O}(\alpha k^2) \pm \frac{i}{2}\sqrt{4B^x k^2 - \alpha^2 + \mathcal{O}(\alpha^2 k^2)} \\ &\approx \frac{1}{2}\alpha \pm \frac{i}{2}\sqrt{4B^x k^2 - \alpha^2},\end{aligned}$$

giving the dispersion relation for the MPFCA model, i.e., Eq. (30). The expansion in α is justified since α has to be small in order to have high wavelength oscillating solutions. The amplitude energy F penalises high k modes and they are rarely seen in the calculations. Modes with $k = 1$ correspond to oscillations at interatomic distance implying that it is a relatively good approximation to state that for the large scale displacements $k \ll 1$.

The reason for studying the simpler MPFCA and AMPFCA models is that they are computationally more efficient than the HPFCA model. First, unlike in the case of full hydrodynamic description, it is possible to leave out the slow density field ρ when the problem does not require local changes in the average density. Second, discarding the velocity field \mathbf{v} saves computer memory and—more importantly—avoids numerical problems associated with systems with advective transport. However, it seems that the long wavelength properties of the MPFCA and AMPFCA models are limited.

The results presented here suggest that while the MPFCA model remains a good qualitative description of fast dynamics, it is not suitable for separating the time scales of the lattice vibrations and the diffusional phenomena. The relaxation

times of grain boundaries and slow phenomena are always coupled through the parameter α to the relaxation of elastic excitations. This should become more important when the system size is increased. The reason for this is that in order to include all the oscillating modes that fit in the spatial domain of the calculation, the MPFCA dissipation parameter α needs to be decreased. On the other hand, decreasing α reduces the overall dissipation in the system slowing any dissipative processes.

ACKNOWLEDGMENTS

This work has been supported in part by the Academy of Finland through its COMP CoE Grants No. 251748 and No. 284621. The authors acknowledge CSC IT Center for Science, Finland, for generous computational resources. We acknowledge the computational resources provided by the Aalto Science-IT project.

APPENDIX A: DERIVATION OF EQ. (20)

Here we expand the free energy F to a quadratic order in the displacement field \mathbf{u} . We write the complex amplitudes as $\eta_j = \phi_0 \exp(-i\mathbf{q}_j \cdot \mathbf{u})$. We assume that the amplitudes of the complex fields are constant. Looking at Eq. (8) we see that only parts where the phase of the complex fields matter are the parts with the operator \mathcal{G}_j and the terms $\eta_1 \eta_2 \eta_3$ and its complex conjugate. The latter terms give

$$\prod_{j=1}^3 \eta_j = \phi_0^3 e^{-i\mathbf{u} \cdot \sum_{j=1}^3 \mathbf{q}_j} = \phi_0^3, \quad (\text{A1})$$

since $\sum_{j=1}^3 \mathbf{q}_j = 0$.

The only remaining part is

$$f_{\text{el}} := B^x \sum_{j=1}^3 |\mathcal{G}_j \phi_0 e^{-i\mathbf{q}_j \cdot \mathbf{u}}|^2. \quad (\text{A2})$$

Using the identity given by Eq. (24) we get

$$\begin{aligned}f_{\text{el}} &= B^x \phi_0^2 \sum_{j=1}^3 |-i\mathbf{q}_j \cdot \mathcal{G}_j \mathbf{u} + \mathcal{O}(|\mathbf{u}|^2)|^2 \\ &= B^x \phi_0^2 \sum_{j=1}^3 |-i\mathbf{q}_j \cdot \nabla^2 \mathbf{u} + 2\mathbf{q}_j \cdot (\mathbf{q}_j \cdot \nabla) \mathbf{u} + \mathcal{O}(|\mathbf{u}|^2)|^2 \\ &= B^x \phi_0^2 \sum_{j=1}^3 \{(\mathbf{q}_j \cdot \nabla^2 \mathbf{u})^2 + 4[\mathbf{q}_j \cdot (\mathbf{q}_j \cdot \nabla) \mathbf{u}]^2 + \mathcal{O}(|\mathbf{u}|^3)\}.\end{aligned} \quad (\text{A3})$$

We take the long-wavelength limit discarding higher-order derivatives and the terms of order higher than two and get

$$f_{\text{el}} \approx 4B^x \phi_0^2 \sum_{j=1}^3 [\mathbf{q}_j \cdot (\mathbf{q}_j \cdot \nabla) \mathbf{u}]^2. \quad (\text{A4})$$

Here it is convenient to use the Einstein summation convention: now

$$f_{\text{el}} \approx 4B^x \phi_0^2 q_{j,i_1} q_{j,i_2} q_{j,i_3} q_{j,i_4} (\partial_{i_1} u_{i_2}) (\partial_{i_3} u_{i_4}). \quad (\text{A5})$$

Here q_{j,i_1} denotes the component i_1 of the vector \mathbf{q}_j . It can be shown that

$$q_{j,i_1} q_{j,i_2} q_{j,i_3} q_{j,i_4} = \frac{3}{8} (\delta_{i_1,i_2} \delta_{i_3,i_4} + \delta_{i_1,i_3} \delta_{i_2,i_4} + \delta_{i_1,i_4} \delta_{i_2,i_3}) \quad (\text{A6})$$

by using Eq. (25) and the fact that $\sum_j \mathbf{q}_j = 0$ (or in coordinates with a lengthy calculation). Now

$$f_{\text{el}} \approx B^x \phi_0^2 \frac{3}{2} [(\partial_{i_1} u_{i_1}) (\partial_{i_3} u_{i_3}) + (\partial_{i_1} u_{i_2}) (\partial_{i_3} u_{i_2}) + (\partial_{i_1} u_{i_2}) (\partial_{i_3} u_{i_1})]. \quad (\text{A7})$$

Using the definition $\epsilon_{ij} = \frac{1}{2} (\partial_i u_j + \partial_j u_i)$, we can recast this in a form

$$f_{\text{el}} \approx \frac{3}{2} B^x \phi_0^2 (\partial_k u_k \delta_{ij} + 2\epsilon_{ij}) \epsilon_{ij}, \quad (\text{A8})$$

from which we recover Eq. (20) using the definition $\boldsymbol{\sigma} : \boldsymbol{\epsilon} = \sigma_{ij} \epsilon_{ij}$.

APPENDIX B: THE IMAGINARY PART OF THE SMALL DISPLACEMENT EQUATION FOR THE AMPFCA MODEL

Let us assume at first that $\eta_j(\mathbf{r}, t) = \phi_j(\mathbf{r}, t) \exp[i\theta_j(\mathbf{r}, t)]$. Now

$$\begin{aligned} \phi_j \frac{\delta F}{\delta \phi_j} &= \phi_j \frac{\partial \eta_j^*}{\partial \phi_j} \frac{\delta F}{\delta \eta_j^*} + \text{c.c.} = \phi_j e^{-i\theta_j} \frac{\delta F}{\delta \eta_j^*} + \text{c.c.} \\ &= \eta_j^* \frac{\delta F}{\delta \eta_j^*} + \text{c.c.} = 2 \text{Re} \left(\eta_j^* \frac{\delta F}{\delta \eta_j^*} \right). \end{aligned} \quad (\text{B1})$$

Next we assume that the displacements are small and that $\eta_j = \phi_0 \exp(-i\mathbf{q}_j \cdot \mathbf{u})$. Inserting Eq. (19) in Eq. (10) gives

$$-i\mathbf{q}_j \cdot (\partial_t^2 \mathbf{u} - \alpha \mathcal{Q}_j^2 \partial_t \mathbf{u}) \phi_0 e^{-i\mathbf{q}_j \cdot \mathbf{u}} = -\frac{\delta F}{\delta \eta_j}, \quad (\text{B2})$$

with the help of Eq. (24). Multiplying by $\mathbf{q}_j \eta_j^*$, taking the imaginary part and summing over j gives Eq. (35), but here we look at the real part. Multiplying by η_j^* and taking the real part gives

$$2\phi_0^2 (\mathbf{q}_j \otimes \mathbf{q}_j) : \nabla \mathbf{u} = \frac{1}{2} \phi_0 \frac{\delta F}{\delta \phi_j} \Big|_{\phi_j = \phi_0} \quad (\text{B3})$$

using Eq. (B1).

Assuming that ϕ_j is constant implies that the chemical potential $\delta F / \delta \phi_j = 0$. Otherwise, ϕ_j would change in time. This implies that the right-hand side of Eq. (B3) is 0. Summing over j gives

$$\mathbf{I} : \nabla \mathbf{u} = \nabla \cdot \mathbf{u} = 0. \quad (\text{B4})$$

The assumption that $\phi_j = \phi_0$ implies that the system is incompressible. Another way to see that $\delta F / \delta \phi_j = 0$ is to calculate

$$\frac{\delta F}{\delta \phi_0} = \frac{\delta F_{\text{el}}}{\delta \phi_0} = 3B^x \phi_0 [2\boldsymbol{\epsilon} : \boldsymbol{\epsilon} + (\nabla \cdot \mathbf{u})^2] = \mathcal{O}(|\nabla \mathbf{u}|^2). \quad (\text{B5})$$

This gives 0 since in the dynamical equations we assume that \mathbf{u} is of linear order.

APPENDIX C: NUMERICAL METHODS

All the calculations were solved using a semi-implicit algorithm [16–18], where the linear terms of the form $\mathcal{L}(\nabla)\psi(\mathbf{r})$ are treated implicitly, while the nonlinear parts are treated explicitly. All the spatial derivatives were computed in k space.

-
- [1] K. R. Elder, M. Katakowski, M. Haataja, and M. Grant, *Phys. Rev. Lett.* **88**, 245701 (2002).
 - [2] K. R. Elder and M. Grant, *Phys. Rev. E* **70**, 051605 (2004).
 - [3] H. Emmerich, H. Löwen, R. Wittkowski, T. Gruhn, G. I. Tóth, G. Tegze, and L. Gránásky, *Adv. Phys.* **61**, 665 (2012).
 - [4] P. Stefanovic, M. Haataja, and N. Provatas, *Phys. Rev. Lett.* **96**, 225504 (2006).
 - [5] P. Galenko, D. Danilov, and V. Lebedev, *Phys. Rev. E* **79**, 051110 (2009).
 - [6] S. Majaniemi and M. Grant, *Phys. Rev. B* **75**, 054301 (2007).
 - [7] S. Majaniemi, M. Nonomura, and M. Grant, *Eur. Phys. J. B* **66**, 329 (2008).
 - [8] A. Baskaran, A. Baskaran, and J. Lowengrub, *J. Chem. Phys.* **141**, 174506 (2014).
 - [9] G. I. Tóth, L. Gránásky, and G. Tegze, *J. Phys.: Condens. Matter* **26**, 055001 (2013).
 - [10] S. Praetorius and A. Voigt, *J. Chem. Phys.* **142**, 154904 (2015).
 - [11] V. Heinonen, C. V. Achim, J. M. Kosterlitz, S.-C. Ying, J. Lowengrub, and T. Ala-Nissila, *Phys. Rev. Lett.* **116**, 024303 (2016).
 - [12] N. Goldenfeld, B. P. Athreya, and J. A. Dantzig, *Phys. Rev. E* **72**, 020601 (2005).
 - [13] B. P. Athreya, N. Goldenfeld, and J. A. Dantzig, *Phys. Rev. E* **74**, 011601 (2006).
 - [14] V. Heinonen, C. V. Achim, K. R. Elder, S. Buyukdagli, and T. Ala-Nissila, *Phys. Rev. E* **89**, 032411 (2014).
 - [15] A. Adland, Y. Xu, and A. Karma, *Phys. Rev. Lett.* **110**, 265504 (2013).
 - [16] G. Tegze, G. Bansk, G. I. Tóth, T. Pusztai, Z. Fan, and L. Gránásky, *J. Comput. Phys.* **228**, 1612 (2009).
 - [17] B. P. Vollmayr-Lee and A. D. Rutenberg, *Phys. Rev. E* **68**, 066703 (2003).
 - [18] J. Zhu, L. Q. Chen, J. Shen, and V. Tikare, *Phys. Rev. E* **60**, 3564 (1999).